Design of a Miniature Axial-Flux Spindle Motor With Rhomboidal PCB Winding

Mi-Ching Tsai and Liang-Yi Hsu

Department of Mechanical Engineering, National Cheng Kung University, Tainan 701, Taiwan, R.O.C.

Size reduction has become one of the most important aspects of motor design. This paper presents a miniature axial-flux spindle motor with a rhomboidal printed circuit board (PCB) winding. The design of its mechanical structure aims to eliminate any unnecessary space. Prior to prototyping, the motor geometry is calculated using an approximate analytical model, which helps speed up the design process. The flexible PCB winding represents an ultrathin electromagnetic exciting source where coils are wound in a rhomboidal shape in order to reduce the end-winding length and minimize the copper loss. The design process also incorporates finite-element analysis for further performance evaluation and refinement. The proposed motor is prototyped, and excellent agreement is found between simulation and measurement.

***Index Terms*—Axial-flux spindle motor, motor design, printed circuit board (PCB) winding.**

I. Introduction

RECENTLY, high efficiency and compact size of spindle motors has been demanded by hard disk manufacturers. In the past, these requirements could be satisfied by conventional radial-flux motors. As the drive specification has become more demanding, it has been difficult to design a radial-flux motor that can achieve the required decrease in thickness. For this reason, the axial-flux spindle motor has become a more suitable choice for this application due to its low profile [1]. As discussed in [2], this type of motor structure consists of windings which are fixed below a flat multipole magnet with flux return via a plate above the permanent magnet (PM). The base-plate below the windings is a thin base plate. Axial-flux motors tend to be designed with air-gap windings, i.e., without any teeth or slots, in order to suppress the cogging torque. However, the axial-flux structure does result in an attractive magnetic force between rotor magnets and stator backplate, which increases the bearing friction and affects the running stability of motors.

This paper aims to overcome the disadvantages of the conventional spindle motors in miniature manufacturing. The axial-flux spindle motor shown in Fig. 1 is proposed, where the stator is composed of the shaft, bearing, base plate, and printed circuit board (PCB) winding. The slotless base plate is used to avoid cogging torque, and the PCB winding is designed to achieve an ultrathin motor. As illustrated in Fig. 1, there are six rhomboidal coils in the stator, and the rotor consists of the yoke and the eight-pole PM. Prior to prototyping, a full assessment of the electromagnetic design to calculate the geometrical parameters is essential. To speed up the design process, an analytical technique is first applied to estimate the flux density and decide the suitable parameters. Finite-element analysis (FEA), using ANSOFT Maxwell software [3], is then applied to refine the calculations and validate the analytical design. In this paper, the design objective is to achieve the desired backEMF subject to the space constraint and flux saturation. The design process and analysis are detailed below and completed with the results of the prototype testing.

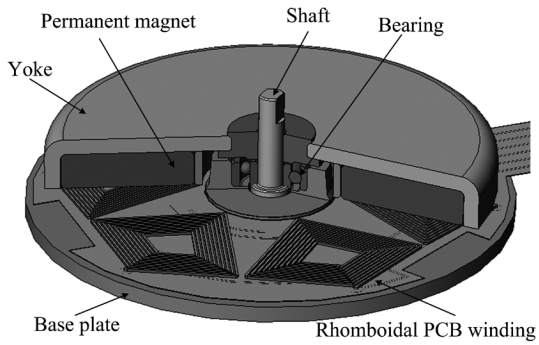

Fig. 1. Structure of the proposed spindle motor.

TABLE I
REQUIREMENTS FOR THE SPINDLE MOTOR

Parameters	Limits
Thickness of motor [mm]	≤ 3.0
Exterior diameter of motor [mm]	≤ 20
Back-EMF constant [mV/(radsec^{-1})]	≥ 0.1

II. Electromagnetic Design

Before design of the motor, specifications regarding the sizing limits and the backEMF constant are listed in Table I. Note that the backEMF constant (k_E) can be determined from the rms open-circuit phase backEMF (E_q) and angular speed (ω)

$$k_E = \frac{E_q(\text{rms})}{\omega}. \tag{1}$$

This leads to $k_T/k_E = 3$ where the torque constant k_T is defined as the torque per amp of phase current [mNm/A(rms)] [4].

In the design procedure, the number of turns per coil (N_c), the stator base-plate thickness (w_p), the rotor yoke thickness (w_y), the permanent magnet thickness (h), and the effective air-gap length (g) are the design variables. An analytical method, which is derived from a simplified two-dimensional model [5], is applied to calculate the flux density. Let R_i and R_a denote the exterior and interior radii of permanent magnets, respectively.

Digital Object Identifier 10.1109/TMAG.2006.879438

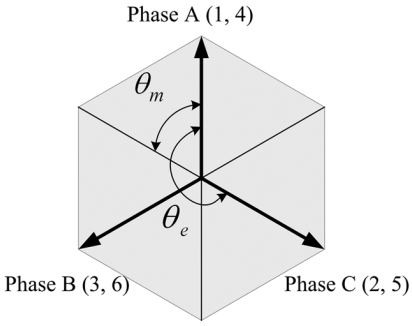

Fig. 2. Star drawing used to determine the connecting of the motor.

The flux passing the cross area of air-gap (A_g) at any angular position θ can be obtained by solving Laplace's equation

$$\Phi_g(\theta) = -4R_a A_g M \times \sum_{n=1,3,5\ldots}^{\infty} \frac{(-1)^{\frac{(n-1}{2}}}{(n\pi)^2 K(n,h,g,R_a)} \sinh(n\alpha)\cos(4n\theta) \quad (2)$$

where

$$K(n,h,g,R_a) = \cosh(n\alpha) - \sinh(n\alpha)\coth(n\beta) \quad (3)$$

$$R_a = \frac{\pi(R_i + R_o)}{8} \quad (4)$$

$$\alpha = \frac{g\pi}{R_a} \quad (5)$$

$$\beta = \frac{(g-h)\pi}{R_a} \quad (6)$$

and M is the magnetization, which relates to the field strength and flux density of the permanent magnets. The design constraints for determining the yoke thickness are given as follows:

$$1 \le \frac{B_{\max} w_y (R_o - R_i)}{\Phi_g(\theta)} \le \frac{3}{2} \quad (7)$$

$$1 \le \frac{B_{\max} w_p (R_o - R_i)}{\Phi_g(\theta)} \le \frac{3}{2} \quad (8)$$

where $B_{\max}$ refers to the allowable flux density in the back plate and yoke. Using these design constraints and the solution of the Laplace equation in (2), the main design parameters of the motor can be obtained. The air-gap length is found to be 0.4 mm, and the maximum air-gap flux density is 0.54 T. Details of the winding structure, including connections and coil shape, can now be addressed. The coils should be distributed as evenly and uniformly around the air-gap surface of the PCB. The mechanical angle (θ_m) and electrical angle (θ_e) of the motor are illustrated in Fig. 2. Note that the machine has eight poles so that $240^\circ\,\text{elec} = 60^\circ\,\text{mech}$. Each coil is then separated based on θ_m, and the phase polarity of the coils is defined by θ_e. There are six concentrated coils, and their connection is illustrated in Fig. 3. The phase sequence in Fig. 3 gives the correct phase polarity and rotation. To achieve higher efficiency, the design adopts rhomboidal-shaped coils to reduce the end windings such that the copper loss can be decreased. The number of turns per coil (N_c) is chosen to be 10 which gives a winding factor of 0.866. Table II summarizes the major motor parameter specification.

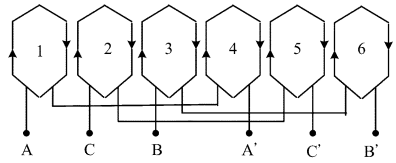

Fig. 3. Winding connections.

TABLE II
MAJOR DESIGN PARAMETERS OF THE SPINDLE MOTOR

Motor Parameter	Designed Value
Thickness of motor [mm]	3.0
Exterior diameter of motor [mm]	17.0
Number of turns per coil [turns]	10
Thickness of plate [mm]	0.6
Thickness of yoke [mm]	0.5
Thickness of PM [mm]	1.4
Exterior radius PM [mm]	7.9
Interior radius PM [mm]	2.9
Thickness of air gap [mm]	0.4
Back-EMF constant [mV/(radsec^{-1})]	0.124

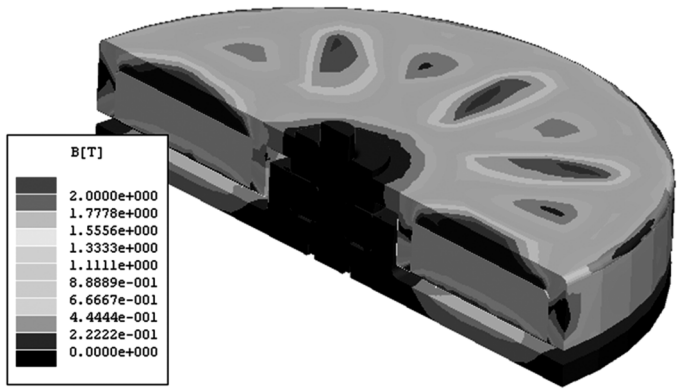

Fig. 4. Distribution of flux density determined by FEA.

A three-dimensional finite-element analysis is employed to calculate the flux density distribution in the steady-state as illustrated in Fig. 4. The FEA confirms the design and shows the effectiveness of the analytical model. Local "hot-spots" in the flux density appear in the rotor yoke above the interpole regions. These suggest that the yoke is the right thickness. Fig. 5 shows the sinusoidal open-circuit backEMF waveforms induced into the phases at a speed of 12 555 rpm. Also, the simulated result shows a 120° elec phase difference between any two of the three phase windings. This confirms the correctness of the winding connection. It can be found that the peak backEMF is 0.23 V, which gives a backEMF constant of 0.124 mV/(radsec^{-1}). This meets the required specification in Table I.

III. PROTOTYPING AND DISCUSSION

From the design outlined in the previous section, a prototype is constructed as shown in Fig. 6. This motor is only 3 mm high with an exterior diameter of 17 mm. The motor utilizes the single-layer rhomboidal PCB winding with ten turns per coil, and the cross section of each conductor is 80 μm×70 μm. The

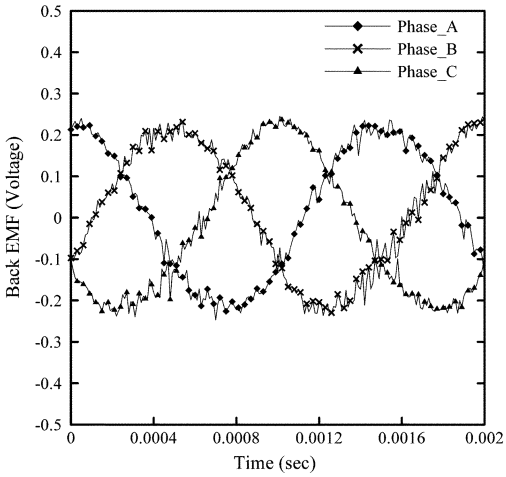

Fig. 5. Predicted backEMF waveforms.

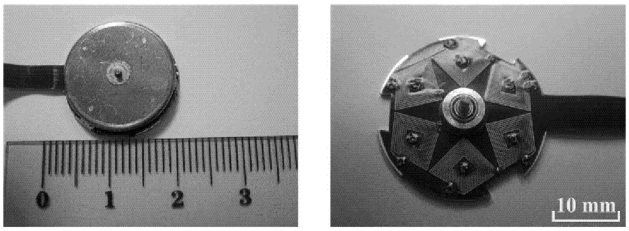

(a) (b)

Fig. 6. Prototyped results. (a) Motor. (b) Rhomboidal PCB winding.

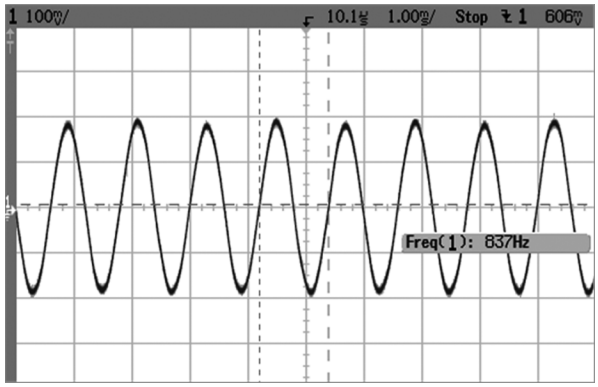

Fig. 7. BackEMF waveform resulted from the prototyped motor.

sintered NdFeB magnet is applied to provide sufficient flux energy. The ultrathin machine structure means excessive copper loss needs to be avoided. The thin conductor cross section can minimize additional eddy-current losses in the winding, particularly for an eight-pole machine operating at high speed. Hence, the rhomboidal winding shape with no end-winding region is advantageous; here, the phase resistance is measured as 3 Ω/m.

Fig. 7 shows the open-circuit backEMF waveforms which are measured at 12 555 rpm. The machine is driven using another machine connect to the shaft. The peak value of backEMF is 0.2 V which means that the backEMF constant is 0.107 mV/(radsec $^{-1}$). This is 13% less than the simulated result but still within the design constraint in Table I. Note that the differences are likely to be due to mechanical tolerances

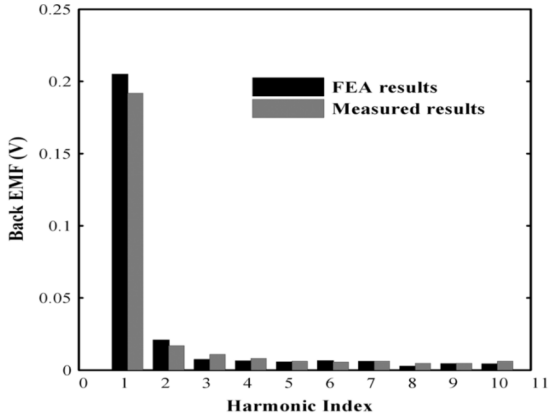

Fig. 8. Comparisons of backEMF between FEA and measured results.

and differences between the simulated and fabricated cases; there may also be material variance. This result also illustrates that the stator base-plate is thin enough to suppress noticeable and excessive base-plate eddy current (which would lead to a reduction in open-circuit voltage and additional losses). The backEMF waveform was found to be sinusoidal as predicted by the FEA, which leads to smooth torque operation. The harmonic content of the measured and simulated backEMFs are compared in Fig. 8 which illustrates the low harmonic content of the waveforms. Hence, excellent agreement is demonstrated.

IV. Conclusion

This paper has presented a design procedure for an axial-flux spindle motor which has promising applications in 3C (computer, communication, and consumption) as miniature motor drives. The design aims to eliminate much of the structure of a conventional radial-flux machine so that its thickness is only 3 mm and exterior diameter is 17 mm. A rhomboidal PCB winding is applied to reduce the copper loss and also to produce sinusoidal backEMF. A prototype motor is fabricated and the performance tested. Measured results from the prototype motor confirm the validation of the proposed design method.

Acknowledgment

The authors are grateful to the Metal Industries Research and Development Centre of the Republic of China for supporting this research.

References

[1] G. H. Jang and J. H. Chang, "Development of dual air gap printed coil BLDC motor," *IEEE Trans. Magn.*, vol. 35, no. 3, pp. 1789–1792, May 1999.

[2] G. H. Jang and J. H. Chang, "Development of an axial-gap spindle motor for computer hard disk drivers using PCB and dual air gaps," *IEEE Trans. Magn.*, vol. 38, no. 5, pp. 3297–3299, Sep. 2002.

[3] Ansoft, *Maxwell 2-D Field Simulation, Release Notes*. Pittsburgh, PA: Ansoft Corp., 2001.

[4] D. C. Hanselman, *Brushless Permanent-Magnet Motor Design*. New York: McGraw-Hill, 1994.

[5] E. P. Furlani, "A method for predicting the field in permanent-magnet axial-field motors," *IEEE Trans. Magn.*, vol. 28, no. 5, pp. 2061–2066, Sep. 1992.

Manuscript received March 9, 2006 (e-mail: mctsai@mail.ncku.edu.tw).